nature photonics

Article

https://doi.org/10.1038/s41566-024-01565-1

Optical pumping of electronic quantum Hall states with vortex light

Received: 15 January 2024

Accepted: 8 October 2024

Published online: 26 November 2024

Check for updates

Deric Session[1,10], Mahmoud Jalali Mehrabad[1,10] ✉, Nikil Paithankar[2,10], Tobias Grass[3,4], Christian J. Eckhardt[5,6], Bin Cao[1], Daniel Gustavo Suárez Forero[1], Kevin Li[1], Mohammad S. Alam[1], Kenji Watanabe[7], Takashi Taniguchi[7], Glenn S. Solomon[8], Nathan Schine[1], Jay Sau[1,9], Roman Sordan[2] & Mohammad Hafezi[1] ✉

A fundamental requirement for quantum technologies is the ability to coherently control the interaction between electrons and photons. However, in many scenarios involving the interaction between light and matter, the exchange of linear or angular momentum between electrons and photons is not feasible, a condition known as the dipole approximation limit. An example of a case beyond this limit that has remained experimentally elusive is when the interplay between chiral electrons and vortex light is considered, where the orbital angular momentum of light can be transferred to electrons. Here we present a mechanism for such an orbital angular momentum transfer from optical vortex beams to electronic quantum Hall states. Specifically, we identify a robust contribution to the radial photocurrent, in an annular graphene sample within the quantum Hall regime, that depends on the vorticity of light. This phenomenon can be interpreted as an optical pumping scheme, where the angular momentum of photons is transferred to electrons, generating a radial current, and the current direction is determined by the vorticity of the light. Our findings offer fundamental insights into the optical probing and manipulation of quantum coherence, with wide-ranging implications for advancing quantum coherent optoelectronics.

Coherent manipulation of light–matter hybrids plays a crucial role in advancing future quantum technologies and optoelectronics[1,2]. Particularly desirable is the control over the spatial degree of freedom in light–matter interactions. Typically, owing to the presence of disorder or Coulomb binding, electronic wavefunctions are much more spatially confined than the wavelengths of associated optical transitions. Consequently, the light–matter interaction occurs locally, and neither the spatial profile of the optical field nor the spatial extent of the electron wavefunction has a significant influence on these interactions, a regime known as the dipole approximation. In other words, in this regime, only direct optical transitions are accessible, and the transfer of linear and orbital angular momentum (OAM), which enables optical control of the spatial degrees of electrons, is not possible.

To understand this, one can consider a simplified model of a hydrogen-like atom, where the typical Bohr radius (a_B) is much smaller than the corresponding optical transition wavelength (λ). Therefore,

[1]Joint Quantum Institute (JQI), University of Maryland, College Park, MD, USA. [2]L-NESS, Department of Physics, Politecnico di Milano, Como, Italy. [3]DIPC—Donostia International Physics Center, San Sebastián, Spain. [4]Ikerbasque—Basque Foundation for Science, Bilbao, Spain. [5]Institut für Theorie der Statistischen Physik, RWTH Aachen University and JARA-Fundamentals of Future Information Technology, Aachen, Germany. [6]Max Planck Institute for the Structure and Dynamics of Matter, Center for Free-Electron Laser Science (CFEL), Hamburg, Germany. [7]National Institute for Materials Science, Tsukuba, Japan. [8]Department of Physics and the Institute of Photonics and Advanced Sensing (IPAS), University of Adelaide, Adelaide, South Australia, Australia. [9]Condensed Matter Theory Center, University of Maryland, College Park, MD, USA. [10]These authors contributed equally: Deric Session, Mahmoud Jalali Mehrabad, Nikil Paithankar. ✉e-mail: mjalalim@umd.edu; hafezi@umd.edu

https://doi.org/10.1038/s41566-024-01565-1

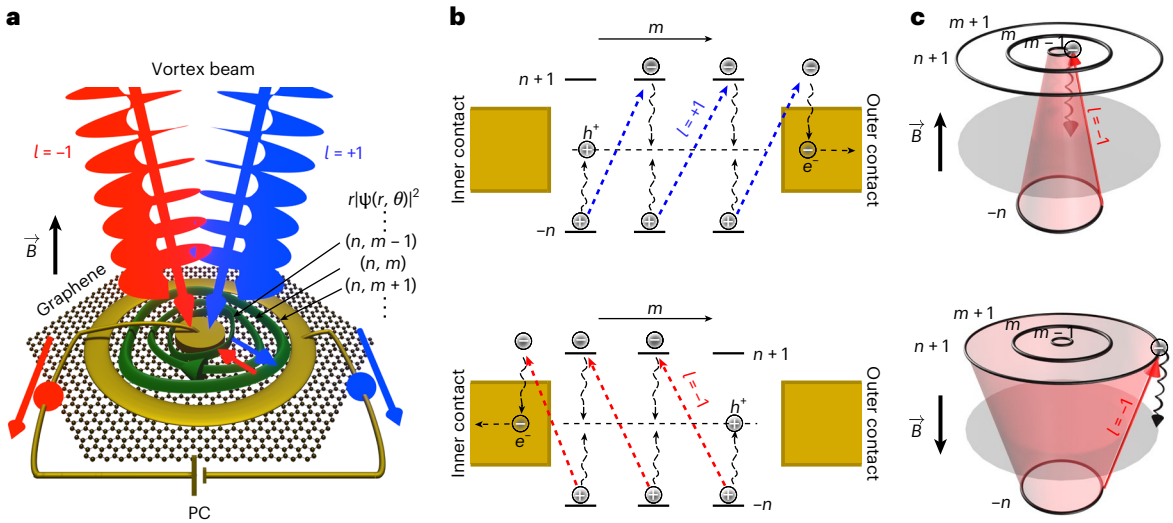

Fig. 1 | Concept of OAM pumping. a, Schematic of LLs in the annular disc geometry subject to the vertically irradiated vortex beam. The green surfaces show representative states within a single LL. The electron distributions in the lowest LLs and directions of the induced radial PC are indicated by arrows. **b**, Optical transitions and PC generation between inner and outer contacts using $\ell = +1$ (blue arrows) and $\ell = -1$ (red arrows) for σ^+ polarized light. For σ^- transitions, see Supplementary Section 7. Light carrying OAM $\ell = +1$ ($\ell = -1$) increases (decreases) m and hence leads to expansion (shrinking) of the spatial extent of the electronic wavefunction. In this way, the shown scheme realizes an analogue to optical pumping. **c**, Schematic of the photoexcitation transitions between LLs with negative (red arrow) vortex beam in the presence of an upward (top) and downward (bottom) pointing magnetic field. In the top (bottom) panel, the magnetic field is anti-parallel (parallel) to the helicity of light, leading to the shrinking (expansion) of the wavefunction radius. In **c**, only the electron relaxation is considered.

the next-order quadrupole transition is weaker by a factor of $(a_B/\lambda)^2$ than the dipole transition, yet it is still observable in ion trap experiments where ions are excited with OAM beams[3]. In fact, in the dipole approximation regime, most of the imparted angular momentum goes to the centre of mass[4–6] and leads to stirring. Such an effect has been observed both in neutral cold atoms[7] and exciton–polariton systems[8–10].

One approach to go beyond the dipole approximation limit is to shrink the wavelength of the electromagnetic field, which can be achieved by using plasmonic effects[11,12]. Alternatively, if the electronic wavefunction is coherently extended over the associated optical transition wavelength, and electrons are more itinerant than bound, then a gross violation of the dipole approximation is expected. For the case of linear excitation, this can lead to the photon drag effect if the electron–hole binding is weak[13]. The other striking example is the quantum Hall system, where the electrons in two dimensions are subject to a strong out-of-plane magnetic field. Consequently, the kinetic energy is suppressed and electrons exhibit cyclotron motions with chiral characteristics that make it a promising system to investigate the interplay of the chirality of electrons and photons and the transfer of angular momentum in between[14–18].

In particular, there has been a growing interest in investigating chiral and topological effects in photonic systems and also light–matter hybrids[18–21]. Such topological features can be either in the momentum domain and lead to Chern bands, or simply in the spatial degrees of freedom, such as optical vortex beams. Specifically, in addition to spin, in the form of polarization, light can also carry OAM[22,23]. Such an OAM is quantized and given by $\hbar\ell$, where $\hbar$ is the Dirac constant and ℓ is the mode number that determines the phase winding of a vortex beam. The interaction of such vortex beams with materials has led to a plethora of exciting phenomena[24], such as the orbital photogalvanic effect[25]. So far, such studies have not been extended to the quantum Hall regime.

In this work, we experimentally demonstrate the transfer of OAM to electrons in a quantum Hall graphene device with annular geometry using optical vortex beams. In particular, harnessing non-conventional optical selection rules of the Landau levels (LLs) described in Fig. 1c, we show a vorticity-selective light–matter interaction between twisted light and the electronic wavefunctions manifesting as a radial photocurrent (PC). We show that this radial PC only depends on the vorticity of light as a direct indication of spatially coherent light–matter interaction. We provide further evidence of the robustness of this mechanism by comparison with circularly polarized light. Specifically, we find that the PC contribution from OAM is at least one order of magnitude larger than the contribution of spin angular momentum (polarization), allowing us to confirm the significant role of the beam's spatial topology, and its ability to control the spatial degree of electrons.

To present the motivation and a basic understanding of our experiment, we discuss spatially dependent light–matter interactions that can manipulate the spatial degrees of freedom of electrons within a quantum Hall system. In particular, using an LL picture, we observe how the transfer of OAM from photons to electrons results in a radial current, where the direction of the current is determined by the vorticity of the light. As shown in Fig. 1, we consider optical transitions between two LLs, in the presence of rotational symmetry perpendicular to the plane of the quantum Hall sample. In this scenario, the sample is irradiated by an optical vortex where each photon is carrying an OAM $\hbar\ell$ (refs. 14,16).

During the excitation process, the OAM of $\hbar\ell$ is transferred to electrons[14,16]. As the radius of the electronic wavefunction increases monotonically with angular momentum, this optical transfer of angular momentum causes a radial change in the electronic wavefunction, which is solely determined by the vorticity of the light. The subsequent relaxation process conserves OAM on average and therefore maintains the OAM transfer from the original excitation. This concept is in direct analogy to optical pumping in atomic systems, wherein cyclical pumping among different hyperfine states of bound electrons within an atom transfers them to a specific quantum state[26].

Note that despite the absence of rotational symmetry in the presence of disorder, the optical pumping model continues to hold true[16]. Moreover, the optical pumping picture also provides a simple estimate of the resulting PC: assuming that OAM pumping was the only mechanism of charge transport, the OAM needed to carry one electron through the sample equals the number M of orbitals in an LL, which is given by $M = A/(\pi l_B^2)$, where A is the area of the sample and l_B is the magnetic

https://doi.org/10.1038/s41566-024-01565-1

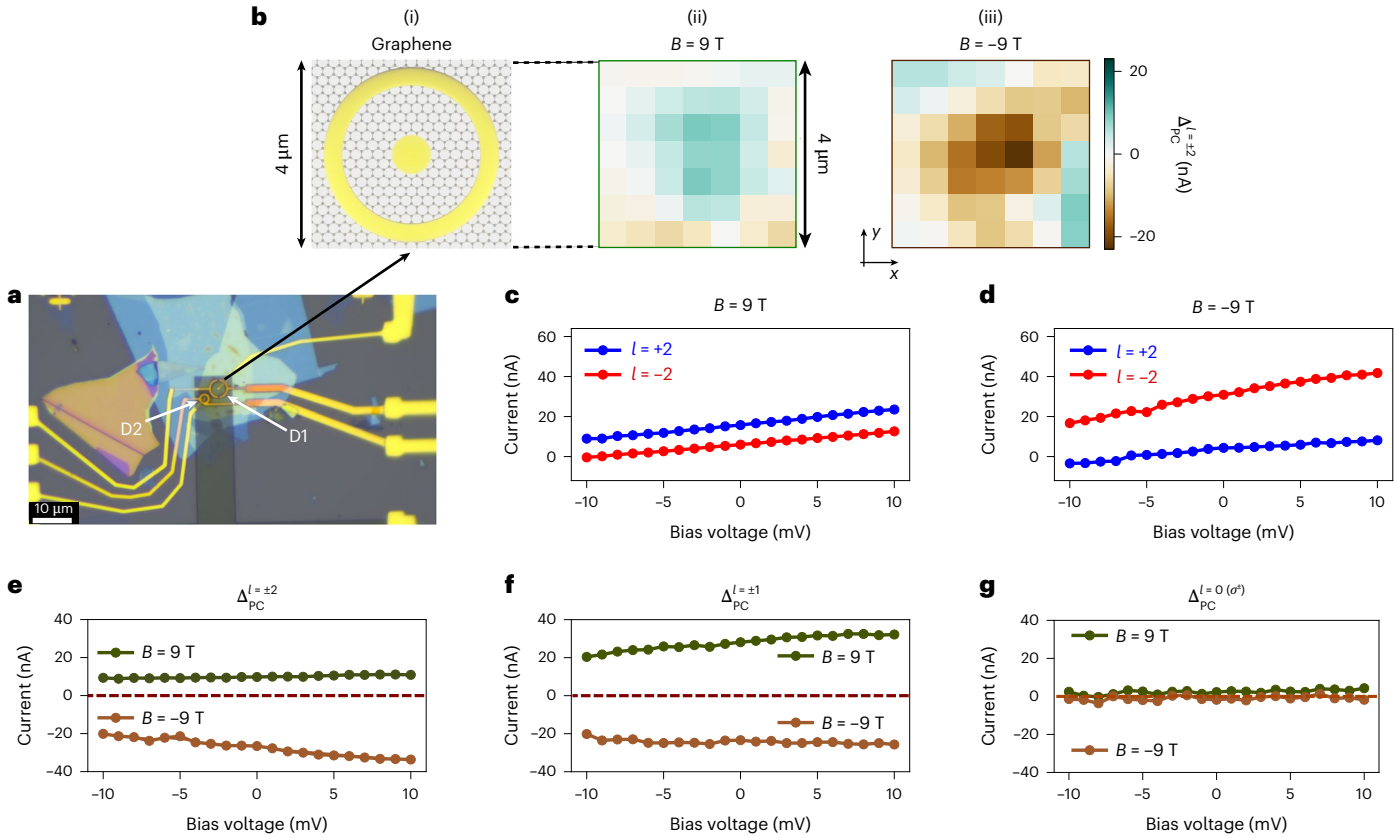

Fig. 2 | OAM-selective PC generation. a, Optical microscope image of the sample, showing two Corbino devices labelled D1 and D2. Corbino D1 has a diameter of ~4 μm and Corbino D2 has a diameter of ~2 μm. D1 is the device used for the data in the main text of this article, for which the inner and outer contacts are marked. The grey rectangle shows the metallic back gate. **b**, (i) Sample schematic and (ii,iii) spatially resolved PC difference Δ_{PC} for $\ell = \pm 2$, at $B = 9$ T and $B = -9$ T, respectively. Bias voltage V_b for both cases was −4 mV. **c**,**d**, Measured PC as a function of bias voltage V_b generated using light carrying $\ell = +2$ (blue) and $\ell = -2$ (red) at $B = 9$ T (**c**) and $B = -9$ T (**d**). **e**–**g**, The Δ_{PC} for $B = 9$ T (green) and $B = -9$ T (brown) for $\ell = \pm 2$ (**e**), $\ell = \pm 1$ (**f**) and $\ell = 0$ (**g**), respectively. In **g**, at each magnetic field, the Δ_{PC} is calculated by subtracting the PC generated using two Gaussian beams with opposite circular polarization ($\sigma^{\pm}$). In all panels, the gate voltage V_g and the average pump power were 1.78 V and 10 μW, respectively. Relative differences of curves within and between **e** and **f** depend on system parameters, which are described in Supplementary Section 4a.

length. The estimated transported charge, δQ, during the time interval δt by N_{ph} photons, is $\delta Q = eN_{ph}\ell/M$. Therefore, for photons with energy $\hbar\omega$, the PC obtained from the laser power $P = \hbar\omega \times N_{ph}/\delta t$ is $I = \delta Q/\delta t = eP\ell/(\hbar\omega M)$. This picture also implies that, upon inverting the direction of the magnetic field, the PC changes direction, as illustrated in Fig. 1c.

Results

Bias voltage dependence of PC

To experimentally demonstrate this mechanism, we use a device consisting of a hexagonal boron nitride (hBN) encapsulated monolayer graphene in an annular (Corbino) geometry as shown in Fig. 2a. The choice of the Corbino geometry allows us to exclusively probe the transport of bulk states. Moreover, the circularly symmetric shape of the Laguerre–Gauss mode profiles optically matches the shape of the sample. The inner and outer contacts are used to apply an in-plane electric field and also measure the generated PC, while the back-gate voltage V_g controls the Fermi level. We apply an out-of-plane external magnetic field up to 9 T at 4.2 K to be in the quantum Hall regime. The optical vortex beams of different vortices ℓ are generated by a spatial light modulator (SLM) and are concentrically focused on the Corbino device (for the sample and optical set-up, see Supplementary Sections 1 and 3). This enables us to excite the carriers in our device, which undergo vorticity-selective optical transitions, shown in Fig. 1c. For all the measurements, we choose $V_g = 1.78$ V, which sets the Fermi energy near filling factor $\nu = 6$.

The generated PC for various optical vortices $\pm\ell$ are independently measured, while the beam is spatially scanned over the sample. Figure 2b shows PC difference (subtracted), Δ_{PC}, where the vortex beam $\ell = \pm 2$ is spatially scanned over the sample (shown schematically in (i)), at (ii) $B = 9$ T and (iii) $B = -9$ T. It can be clearly observed that the Δ_{PC} flips sign when the magnetic field direction is reversed. This remarkable observation corroborates with the earlier optical pumping picture of Fig. 1a, where depending on the vortices of the optical beam the radial extent of the electrons either shrink or expand during the optical excitation. Note that the sign of the observed PC difference depends solely on the phase winding of the optical vortex beam, and not the intensity; therefore, one cannot associate this (beyond the dipole approximation) process with heating.

It is unlikely that any sample has pristine electrical conditions and it may harbour residual or intrinsic in-plane potential. Such inherent potential could potentially explain the presence of a radial PC in the Corbino sample. To rule out the origin of our observed effect to such an in-plane electric field, we apply a bias voltage V_b between the inner and outer contacts to create a controllable potential gradient in the radial direction. Figure 2c,d shows the measured PC as a function of V_b for $B = 9$ T and $B = -9$ T, respectively. Remarkably, we observe multiple unambiguous signatures of the vorticity-selective light–matter interaction. First, as shown in Fig. 2c,d, for $\ell = +2$ (blue) and $\ell = -2$ (red) at each magnetic field, we observe a consistent and significant difference in the generated PC for a wide range of V_b ($-10 \le V_b \le 10$ mV). In other

https://doi.org/10.1038/s41566-024-01565-1

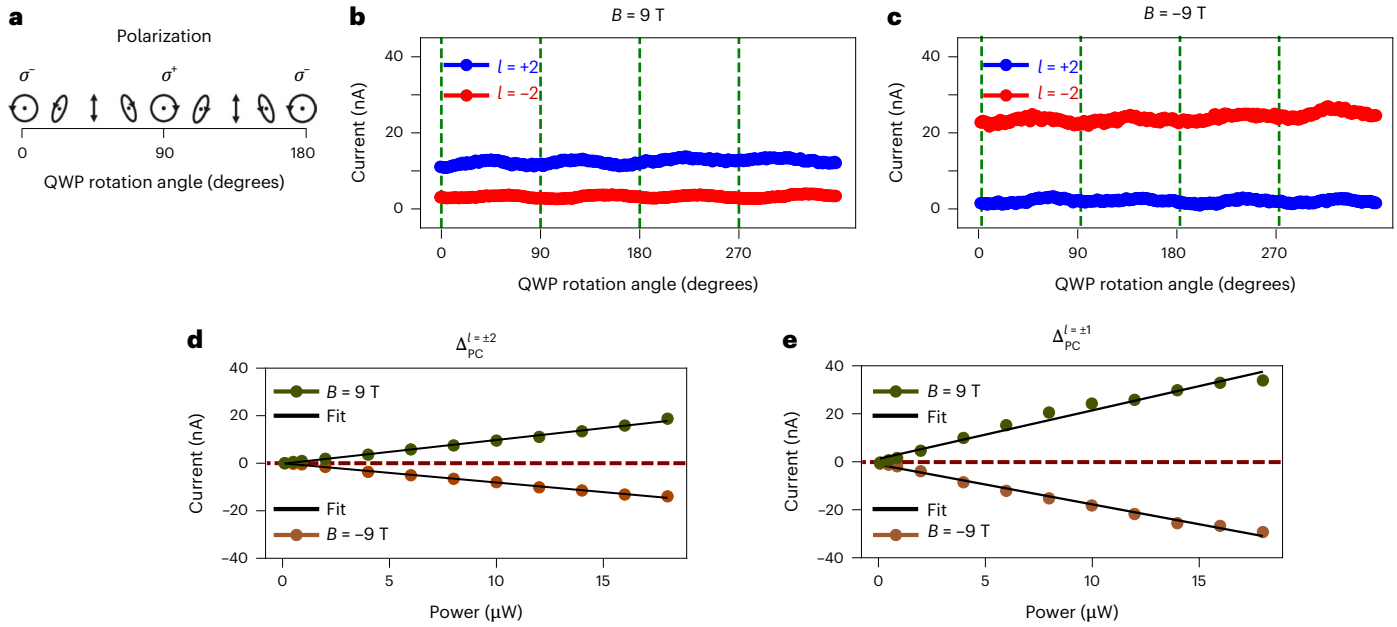

Fig. 3 | Polarization-resolved and power-dependent PC measurements. **a**, Polarization of the pump beam as a function of the QWP rotation, shown schematically at the top. σ^+ and σ^- denote the positive and negative circular polarization. Between each consecutive circular polarization, continuous rotation of the QWP changes the polarization periodically from circular to elliptical, to linear polarization. **b**,**c**, PC measured as a function of QWP rotation using light carrying $\ell = +2$ (blue) and $\ell = -2$ (red) at $B = 9$ T (**b**) and $B = -9$ T (**c**), respectively. The green vertical dashed lines indicate the consecutive σ^+ and σ^- polarization. All measurements are done at a fixed $V_g = 1.78$ V, $V_b = -4$ mV and an average pump power of 10 μW. **d**,**e**, Pump power dependence of PC: PC difference Δ_{PC} measured as a function of average pump power using light carrying $\ell = \pm 2$ (**d**) and $\ell = \pm 1$ (**e**) OAM at $B = 9$ T (green circles) and $B = -9$ T (brown circles), respectively. The black lines show the least-squares linear fit. In all of the data presented in the main text, the average pump power was set to 10 μW, at which a linear behaviour is observed.

words, radially tilting the electric potential can change the total PC; however, the PC difference Δ_{PC} remains relatively constant. Second, for the opposite magnetic field, we observe a clear sign flip for the PC difference (Fig. 2e). Specifically, since the OAM is defined relative to the magnetic field, inverting the latter effectively inverts the OAM and should therefore lead to a sign change of the observed radial PC, which is clearly observed in Fig. 2e. In an ideal case, the amplitude of this flipped current should be the same; however, owing to slightly different spatial alignment for different magnetic fields, the magnitude of the PC is different (Fig. 2b, (ii) and (iii)). Third, to investigate the effect of the degree of vorticity on the generated PC, we illuminate the sample with $\ell = \pm 1$ beams. As shown in Fig. 2, robust PC difference $\Delta_{PC}^{\ell=\pm1}$ is observed across a wide range voltage bias, and the sign reversal with the magnetic field is present. For a large sample subject to the optical vortex, one expects Δ_{PC} to increase with the vorticity degree ℓ (ref. 16). However, we note that our experiment was designed such that the Corbino sample would have an optimal spatial overlap for optical vortex beams with $\ell = \pm 1$. Since the OAM beams with larger vorticity are spatially larger (in free space, the vortex of the OAM beam with $\ell = \pm 2$ is approximately two times larger than that of the beam with $\ell = \pm 1$), the spatial overlap of the sample and optical vortex beam reduces with vorticity. This means that the amount of graphene inside the Corbino that is illuminated decreases with vorticity. This reduction of beam-sample overlap is the main reason why we observe a reduced Δ_{PC} for $\ell = \pm 2$ compared with $\ell = \pm 1$. Moreover, as shown in Fig. 2b, the magnitude of radial PC difference, Δ_{PC}, diminishes as the centre of the beam reaches the outer contact. This indicates that graphene-contact interface effects are not playing a significant role in our observations and the radial PC is dominantly generated from the bulk.

Fourth, to rule out the origin of Δ_{PC} based on circular polarization, the sample is illuminated with $\ell = 0$ beams consisting of two Gaussian beams with opposite circular polarization (σ^+ and σ^-). As shown in Fig. 2g, the PC difference for different circular polarization and $\ell = 0$ is at least an order of magnitude smaller than the non-zero ℓ cases. Therefore, we associate the non-zero radial current with the OAM of light, rather than the spin angular momentum.

Polarization dependence of PC

To further decouple the role of the polarization of the optical field from OAM in our experiments, we perform polarization-resolved PC generation using OAM of light by using a variable quarter-wave plate (QWP) in the excitation path. We rotate the QWP such that the polarization continuously changes from linear to elliptical to circular while measuring the PC (Fig. 3a). The measured PC for $\ell = +2$ (blue) and $\ell = -2$ (red) at $B = 9$ T and $B = -9$ T is shown in Fig. 3b,c.

Here there are three clear observations confirming the robustness of OAM-induced PC generation. First, the OAM-induced PC difference is almost an order of magnitude larger than the amplitude of the current oscillations induced by QWP rotation. Second, the OAM-induced PC difference never changes sign as a function of QWP rotation, further confirming the domination of the observed vorticity-selective PC. Finally, this measurement sheds light on the role of focusing the optical beam on its polarization properties. This is crucial since in our measurements, we focus the beam onto the sample using an aspheric lens with a numerical aperture (NA) of 0.68. This large NA may distort the polarization beyond the paraxial approximation. However, Fig. 3b,c shows that this distortion of polarization is relatively insignificant and it does not affect the validity of our results.

Power dependence of PC

To verify the linear power dependence of the OAM transfer, we also investigate the power dependence of the OAM-induced PC in our measurements as a function of optical pump power by varying the average power of our excitation beam within the range of 0.1–18 μW. Figure 3d,e shows that the generated PC increases linearly with the pump intensity. From the above optical pumping estimate, we have

https://doi.org/10.1038/s41566-024-01565-1

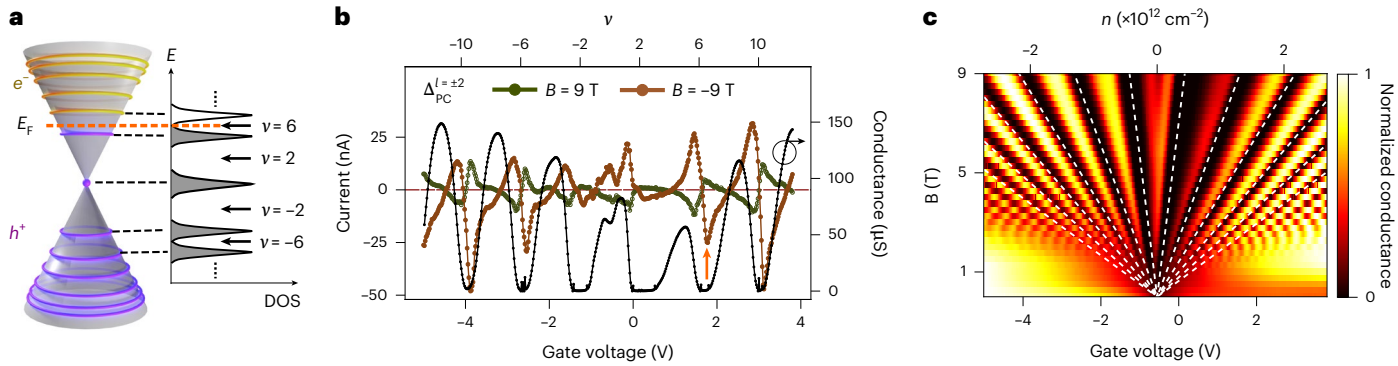

Fig. 4 | Gate voltage dependence of PC. a, Schematic of graphene's band structure near the Dirac point with LLs shown in yellow and purple for the electron and holes, respectively. The inset shows the density of states (DOS) as a function of energy with the Fermi energy. **b**, Measured PC difference as a function of gate voltage using light carrying $\ell = \pm 2$ at $B = 9$ T (green) and $B = -9$ T (brown), respectively. The top x-axis shows the calculated integer filling factors (Supplementary Section 2). The two-terminal longitudinal conductance measured at $B = 9$ T (black circles) is also shown. This measurement was done at $V_b = -4$ mV and an average pump power of 10 μW. The orange arrow indicates the gate voltage for which all the previous measurements were performed. **c**, Landau fan measured via magneto-transport as a function of the magnetic field, gate voltage (carrier density marked on the top x-axis). The conductance is normalized for each magnetic field value. The white dashed lines denote integer filling factors calculated from the conversion of gate voltage to carrier density (Supplementary Section 2).

$l_B \approx 26\,\text{nm}/\sqrt{B/(1\,\text{tesla})} \approx 9$ nm, and $M = A/(\pi l_B^2) \approx 3 \times 10^4$. The PC is estimated to be $I \approx (0.1\,\text{nA}\,\mu\text{W}^{-1})P$. Interestingly, the slope of the experimental power dependence (~1 nA μW^{-1}) significantly exceeds this estimate. As we discuss in more detail below, the PC signal also shows a strong gate voltage dependence owing to relaxation effects, and the experimental values are taken at local PC difference maxima, where significant carrier multiplication can be expected[27]. In addition, the donut-shaped intensity profile of the light, not taken into account in the estimate, enhances the current flow into the outer contact. In addition, the OAM-induced PC differences increase linearly with pump power, which indicates that our experiment was performed in the linear regime away from the Pauli blockade in ref. 16.

Gate voltage dependence of PC

Next, we investigate the role of the Fermi energy (E_F) in the generated vorticity-selective PC. By changing the gate voltage V_g, we tune E_F between LLs, that is, we tune the LL filling factor ν. As shown in Fig. 4b, the subtracted PC (for $\ell = \pm 2$) changes sign as a function of V_g, with the direction of PC changing twice between each consecutive conductance peak. In Fig. 4b, green (brown) denotes the subtracted PC at $B = 9$ T ($B = -9$ T), respectively. Such a sign change has also been observed in other quantum Hall graphene systems. This phenomenon has been attributed to a 'bottleneck effect' where the location of E_F with respect to the LLs favours the relaxation of electrons versus holes, and therefore the PC can change sign with V_g (ref. 27). While such an effect was observed in a rectangular geometry to explain the chirality of edge PC, it is likely that the bottleneck effect is also changing the majority carriers in the bulk, and therefore it is relevant to our Corbino geometry. Moreover, a semiclassical scattering analysis (Supplementary Sections 10 and 11) shows that the variation of the longitudinal conductivity near the plateau transition can also contribute to a sign change of the PC.

Discussion

In summary, we demonstrated a mechanism for transferring OAM from photons to electrons. Our OAM optical pumping scheme is analogous to cold-atom and ion optical pumping, and can be used to manipulate itinerant electrons. In addition, our results suggest that the control of spatial degrees of freedom in light–matter interactions can become a new and versatile toolbox in solid-state systems. Generally, our OAM-selective optical pumping picture assumes non-interacting electrons and can be extended to other platforms in which the Coulomb binding energy is weak and therefore the excitonic Bohr radius remains larger than the field gradient length scale. This approach heralds a new ability to image the spatial coherence of electrons, a fundamentally new probe of quantum materials, inaccessible through existing measurements such as multi-port transport and scanning tunnelling microscopy[28]. For example, our work highlights the potential of using structured light as a powerful tool to monitor the spatial coherence of electronic wavefunctions and its modification to quantum Hall plateau transitions as well as thermal effects. One immediate direction is to use THz fields, as opposed to the optical fields used in our case, to excite the two nearest LLs[29]. The advantage of this approach is the absence of cascade relaxation. Also, the influence of gradient fields on the quantum Hall system has been recently observed in the THz domain, suggesting that this platform is a promising candidate[30]. A more ambitious direction involves the strongly interacting limit, where one could exploit the transfer of OAM to probe fractional quantum Hall states and excite and manipulate anyons[31–35].

Moreover, our experiment provides a unique testbed for investigating the interplay between topology and chirality in the interactions between electrons and photons. While our experiment was performed in the low excitation limit, there are several intriguing proposals to use a strong drive field and exploit the spatially coherent light–matter interaction to induce a wider class of topological insulators in electronic systems by using various structured light[23,36–39]. Furthermore, while our graphene system lacks a photoluminescence response, our scheme can be applied to materials where emission from electronic LLs is possible[40], potentially enabling the observation of chiral photon emission. Another promising avenue is the prospect of coherent wavefunction spectroscopy, where interferometric techniques can be integrated into our experimental scheme to measure and modulate the spatial distribution of wavefunction amplitudes and phases[41].

Online content

Any methods, additional references, Nature Portfolio reporting summaries, source data, extended data, supplementary information, acknowledgements, peer review information; details of author contributions and competing interests; and statements of data and code availability are available at https://doi.org/10.1038/s41566-024-01565-1.

References

1. Bloch, J., Cavalleri, A., Galitski, V., Hafezi, M. & Rubio, A. Strongly correlated electron–photon systems. *Nature* **606**, 41–48 (2022).

2. Basov, D., Fogler, M. & García de Abajo, F. Polaritons in van der Waals materials. *Science* **354**, aag1992 (2016).
3. Schmiegelow, C. T. et al. Transfer of optical orbital angular momentum to a bound electron. *Nat. Commun.* **7**, 12998 (2016).
4. Grass, T., Bhattacharya, U., Sell, J. & Hafezi, M. Two-dimensional excitons from twisted light and the fate of the photon's orbital angular momentum. *Phys. Rev. B* **105**, 205202 (2022).
5. Konzelmann, A. M., Krüger, S. O. & Giessen, H. Interaction of orbital angular momentum light with Rydberg excitons: modifying dipole selection rules. *Phys. Rev. B* **100**, 115308 (2019).
6. Quinteiro, G. F. Below-bandgap excitation of bulk semiconductors by twisted light. *Europhys. Lett.* **91**, 27002 (2010).
7. Andersen, M. et al. Quantized rotation of atoms from photons with orbital angular momentum. *Phys. Rev. Lett.* **97**, 170406 (2006).
8. Boulier, T. et al. Injection of orbital angular momentum and storage of quantized vortices in polariton superfluids. *Phys. Rev. Lett.* **116**, 116402 (2016).
9. Dominici, L. et al. Interactions and scattering of quantum vortices in a polariton fluid. *Nat. Commun.* **9**, 1467 (2018).
10. Kwon, M.-S. et al. Direct transfer of light's orbital angular momentum onto a nonresonantly excited polariton superfluid. *Phys. Rev. Lett.* **122**, 045302 (2019).
11. Andersen, M. L., Stobbe, S., Sørensen, A. S. & Lodahl, P. Strongly modified plasmon–matter interaction with mesoscopic quantum emitters. *Nat. Phys.* **7**, 215–218 (2011).
12. Rivera, N., Kaminer, I., Zhen, B., Joannopoulos, J. D. & Soljačić, M. Shrinking light to allow forbidden transitions on the atomic scale. *Science* **353**, 263–269 (2016).
13. Wieck, A., Sigg, H. & Ploog, K. Observation of resonant photon drag in a two-dimensional electron gas. *Phys. Rev. Lett.* **64**, 463 (1990).
14. Gullans, M. J., Taylor, J. M., Imamoğlu, A., Ghaemi, P. & Hafezi, M. High-order multipole radiation from quantum Hall states in Dirac materials. *Phys. Rev. B* **95**, 235439 (2017).
15. Takahashi, H. T., Proskurin, I. & Kishine, J.-i Landau level spectroscopy by optical vortex beam. *J. Phys. Soc. Jpn.* **87**, 113703 (2018).
16. Cao, B., Grass, T., Solomon, G. & Hafezi, M. Optical flux pump in the quantum Hall regime. *Phys. Rev. B* **103**, L241301 (2021).
17. Hübener, H. et al. Engineering quantum materials with chiral optical cavities. *Nat. Mater.* **20**, 438–442 (2021).
18. Suarez-Forero, D. G. et al. Spin-selective strong light–matter coupling in a 2D hole gas-microcavity system. *Nat. Photon.* **17**, 912–916 (2023).
19. Ozawa, T. et al. Topological photonics. *Rev. Mod. Phys.* **91**, 015006 (2019).
20. Lodahl, P. et al. Chiral quantum optics. *Nature* **541**, 473–480 (2017).
21. Jalali Mehrabad, M., Mittal, S. & Hafezi, M. Topological photonics: fundamental concepts, recent developments, and future directions. *Phys. Rev. A* **108**, 040101 (2023).
22. Allen, L., Barnett, S. M. & Padgett, M. J. *Optical Angular Momentum* (CRC Press, 2003).
23. Bliokh, K. Y. et al. Roadmap on structured waves. *J. Opt.* **25**, 103001 (2023).
24. Rosen, G. F. Q., Tamborenea, P. I. & Kuhn, T. Interplay between optical vortices and condensed matter. *Rev. Mod. Phys.* **94**, 035003 (2022).
25. Ji, Z. et al. Photocurrent detection of the orbital angular momentum of light. *Science* **368**, 763–767 (2020).
26. Cohen-Tannoudji, C. & Kastler, A. in *Progress in Optics* Vol. 5, 1–81 (Elsevier, 1966).
27. Cao, B. et al. Chiral transport of hot carriers in graphene in the quantum Hall regime. *ACS Nano* **16**, 18200–18209 (2022).
28. Feldman, B. E. et al. Observation of a nematic quantum Hall liquid on the surface of bismuth. *Science* **354**, 316–321 (2016).
29. Scalari, G. et al. Ultrastrong coupling of the cyclotron transition of a 2D electron gas to a THz metamaterial. *Science* **335**, 1323–1326 (2012).
30. Appugliese, F. et al. Breakdown of topological protection by cavity vacuum fields in the integer quantum Hall effect. *Science* **375**, 1030–1034 (2022).
31. Grass, T. et al. Optical control over bulk excitations in fractional quantum Hall systems. *Phys. Rev. B* **98**, 155124 (2018).
32. Knüppel, P. et al. Nonlinear optics in the fractional quantum Hall regime. *Nature* **572**, 91–94 (2019).
33. Ivanov, P. A., Letscher, F., Simon, J. & Fleischhauer, M. Adiabatic flux insertion and growing of Laughlin states of cavity Rydberg polaritons. *Phys. Rev. A* **98**, 013847 (2018).
34. Binanti, F., Goldman, N. & Repellin, C. Spectroscopy of edge and bulk collective modes in fractional Chern insulators. *Phys. Rev. Research* **6**, L012054 (2024).
35. Winter, L. & Zilberberg, O. Fractional quantum Hall edge polaritons. Preprint at https://arxiv.org/abs/2308.12146 (2023).
36. Katan, Y. T. & Podolsky, D. Modulated Floquet topological insulators. *Phys. Rev. Lett.* **110**, 016802 (2013).
37. Bhattacharya, U. et al. Fermionic Chern insulator from twisted light with linear polarization. *Phys. Rev. B* **105**, L081406 (2022).
38. Kim, H., Dehghani, H., Ahmadabadi, I., Martin, I. & Hafezi, M. Floquet vortex states induced by light carrying an orbital angular momentum. *Phys. Rev. B* **105**, L081301 (2022).
39. Bao, C., Tang, P., Sun, D. & Zhou, S. Light-induced emergent phenomena in 2D materials and topological materials. *Nat. Rev. Phys.* **4**, 33–48 (2022).
40. But, D. et al. Suppressed Auger scattering and tunable light emission of Landau-quantized massless Kane electrons. *Nat. Photon.* **13**, 783–787 (2019).
41. Zewail, A. H. Four-dimensional electron microscopy. *Science* **328**, 187–193 (2010).

Publisher's note Springer Nature remains neutral with regard to jurisdictional claims in published maps and institutional affiliations.

Springer Nature or its licensor (e.g. a society or other partner) holds exclusive rights to this article under a publishing agreement with the author(s) or other rightsholder(s); author self-archiving of the accepted manuscript version of this article is solely governed by the terms of such publishing agreement and applicable law.

© The Author(s), under exclusive licence to Springer Nature Limited 2024

Methods

Sample fabrication and preparation

Graphene was exfoliated from natural graphite crystals (HQ Graphene) and hBN was exfoliated from lab-grown[42] or commercial (HQ Graphene) synthetic crystals. A hot pickup technique was used to stack the hBN/graphene/hBN heterostructure, which was then transferred onto a pre-patterned local metallic back-gate made of 3 nm of Cr and 2 nm of Pt[43]. The area for the outer contact was etched using a selective reactive ion etching, which was followed by the evaporation of 50 nm of Au to form the outer contact[44]. Next, a third layer of hBN was dropped on top of the heterostructure to act as an insulating layer between the overlapping parts of the contacts. The same selective etch was used to expose the area for the inner contact and 100 nm of Au was evaporated to make the contact. The fabricated devices were wire-bonded to chip carriers for the electrical and PC measurements.

Measurement set-up

The sample, inside a variable temperature insert (VTI), is mounted on top of a piezoelectric stack, cooled to 4.2 K using liquid helium, and can reach magnetic fields of up to 9 T. The VTI has an optical window on top and a confocal microscope is built above to optically resolve the sample. The pump laser is illuminated through the same window and the laser spot's alignment to the sample can be monitored with the microscope. During measurements, the laser power is constantly monitored with a power meter, and feedback is given to a proportional-integral-derivative loop controlling a laser power control module. For all measurements in the main text and Supplementary Information with the exception of power dependence measurements, the average pump power is kept at 10 μW. To generate beams with OAM, a Gaussian beam is diffracted off of a phase-only SLM showing a pitchfork pattern. For PC measurements, the two sample contacts are connected to a custom-built trans-impedance amplifier (TIA) outside of the cryostat[27]. The outputs of the TIA are connected to a lock-in amplifier (SRS SR860). The pump laser is chopped at a frequency of 308 Hz and the lock-in is frequency-locked to the chopper.

Data availability

All of the data that support the findings of this study are reported in the main text, Supplementary Information and Supplementary Video 1. Source data are available from the corresponding authors on reasonable request.

References

42. Watanabe, K., Taniguchi, T. & Kanda, H. Direct-bandgap properties and evidence for ultraviolet lasing of hexagonal boron nitride single crystal. *Nat. Mater.* **3**, 404–409 (2004).
43. Pizzocchero, F. et al. The hot pick-up technique for batch assembly of van der Waals heterostructures. *Nat. Commun.* **7**, 11894 (2016).
44. Jessen, B. S. et al. Lithographic band structure engineering of graphene. *Nat. Nanotechnol.* **14**, 340–346 (2019).

Acknowledgements

The authors acknowledge fruitful discussions with C. Dean, A. Macdonald, I. Kaminer, I. Ahmadabadi, J. Shabani and P. Yu. This work was supported by AFOSR FA95502010223, ONR N00014-20-1-2325, ARO W911NF2010232, MURI FA9550-19-1-0399, FA9550-22-1-0339, NSF IMOD DMR-2019444, ARL W911NF1920181, Simons and Minta Martin foundations, and EU Horizon 2020 project Graphene Flagship Core 3 (grant agreement ID 881603). T.G. acknowledges financial support from the Agencia Estatal de Investigación (AEI) through Proyectos de Generación de Conocimiento PID2022-142308NA-I00 (EXQUSMI), and that this work has been produced with the support of a 2023 Leonardo Grant for Researchers in Physics, BBVA Foundation. The BBVA Foundation is not responsible for the opinions, comments and contents included in the project and/or the results derived therefrom, which are the total and absolute responsibility of the authors. The BBVA Foundation is not responsible for the opinions, comments and contents included in the project and/or the results derived therefrom, which are the total and absolute responsibility of the authors.

Author contributions

D.S. and M.J.M. performed the experiments and analysed the data. N.P. and R.S. fabricated the graphene sample using hBN from K.W. and T.T. B.C., D.G.S.F., K.L., M.S.A. and G.S.S. contributed to building the measurement set-up and software used for measurements. B.C., M.H. and G.S.S. conceived the idea for the experiment. Theoretical analysis was performed by C.J.E., T.G. and J.S. The results were interpreted by D.S., M.J.M., N.S. and M.H. D.S., M.J.M. and M.H. wrote the paper with input from all authors.

Competing interests

The authors declare no competing interests.

Additional information

Supplementary information The online version contains supplementary material available at https://doi.org/10.1038/s41566-024-01565-1.

Correspondence and requests for materials should be addressed to Mahmoud Jalali Mehrabad or Mohammad Hafezi.

Peer review information *Nature Photonics* thanks Ido Kaminer and the other, anonymous, reviewer(s) for their contribution to the peer review of this work.

Reprints and permissions information is available at www.nature.com/reprints.